Available online at www.sciencedirect.com
ScienceDirect
Scripta Materialia 65 (2011) 300–303
Scripta MATERIALIA
www.elsevier.com/locate/scriptamat

Estimating the stress exponent of nanocrystalline nickel: Sharp vs. spherical indentation

In-Chul Choi,[a] Byung-Gil Yoo,[a] Yong-Jae Kim,[a] Moo-Young Seok,[a] Yinmin Wang[b] and Jae-il Jang[a,*]

[a] *Division of Materials Science and Engineering, Hanyang University, Seoul 133-791, South Korea*
[b] *Physical and Life Sciences Directorate, Lawrence Livermore National Laboratory, Livermore, CA 94550, USA*

Received 7 April 2011; revised 19 April 2011; accepted 22 April 2011
Available online 28 April 2011

To overcome the newly found difficulties in estimating the creep exponent through the popular constant-load, sharp-indentation creep method, we propose here a modified way that involves using a spherical tip. Both sharp and spherical indentation creep experiments were performed on nanocrystalline nickel (~30 nm), which is known to show creep-like behavior at room temperature. The results suggest that nanocrystalline nickel exhibits a strong strain-rate-dependent deformation mechanism, and that spherical indentation creep may produce more reliable data than sharp indentation creep.

Keywords: Nanoindentation; Creep; Nanocrystalline materials; Nickel

The time-dependent plastic deformation behavior of nanocrystalline (nc) metals [1], e.g. creep [2–6], is of great interest from both scientific and engineering viewpoints. An important quantitative measure of the creep curve is the slope of the secondary creep regime, so-called steady-state creep rate $\dot{\varepsilon}$, which is described as [7]:

$$\dot{\varepsilon} = \frac{ADGb}{kT}\left(\frac{b}{d}\right)^{p}\left(\frac{\sigma}{G}\right)^{n}, \quad (1)$$

where A is a dimensionless constant, D is the diffusion coefficient, G is the shear modulus, b is the magnitude of the Burgers vector, k is the Boltzmann constant, T is the absolute temperature, p is the inverse grain size exponent, and n is the stress exponent. Of these parameters, the creep stress exponent n $\left(=\frac{\partial \ln \dot{\varepsilon}}{\partial \ln \sigma}\right)$ is often considered as an useful indicator of the dominant creep mechanism, i.e. $n = 1$ for diffusion creep such as Nabarro–Herring or Coble creep, $n = 2$ for grain boundary (GB) sliding, and $n = 3$–8 for dislocation creep [7].

Creep testing according to standard procedures (e.g. ASTM specification E139-06) requires samples of specific size and geometry, and can be time consuming. In this regard, since the 1950s there have been many attempts to estimate creep behavior through indentation experiments. Indentation creep tests have many advantages—indentation can offer nanometer-scale spatial resolution which is ideal for measuring extremely small plasticities; the testing procedure is simple and easy to set up, and only a small volume of material is needed; and one can probe local creep properties, which is valuable not only for micro-/nanoscale structures and interfaces in electric industries but also for relatively large-scale components such as the weld heat-affected zones where complex microstructure gradients exist. The development of instrumented indentation (especially nanoindentation) in the late 1980s makes it possible to systematically investigate the time-dependent mechanical response by analyzing the indentation load–displacement (P–h) curves without hardness impression observation. As reviewed in Refs. [8,9], a variety of nanoindentation creep approaches have been developed, including constant-displacement (or load-relaxation) testing, constant-loading-rate testing, constant-strain-rate testing and constant-load testing. Among these, the most popular method for estimating the creep stress exponent n in Eq. (1) is the constant-load indentation creep experiment with a sharp tip (e.g. Berkovich or Vickers tips) [4,9–11]. In this technique, an extended dwell is made at a constant peak load and the increase in the penetration depth with holding time is monitored.

* Corresponding author; e-mail: jijang@hanyang.ac.kr

1359-6462/$ - see front matter © 2011 Acta Materialia Inc. Published by Elsevier Ltd. All rights reserved.
doi:10.1016/j.scriptamat.2011.04.031

From the depth increase, the continuous change in the stress (which is converted from hardness H by Tabor's empirical law, $\sigma \sim H/C$, where C is the constraint factor which is typically ~3 for metals [12]) during holding can be estimated. The indentation strain rate $\dot{\varepsilon}_i$ is given as $(dh/dt)h^{-1}$ in which the displacement rate (dh/dt) is often calculated by fitting the displacement–holding time (h–t) curve according to an empirical fitting equation:

$$h(t) = h_0 + At^k + Bt, \quad (2)$$

where h_0 is the displacement at the onset of creep, and A, B and k are fitting constants. For comparison with uniaxial creep data, the indentation strain rate ($\dot{\varepsilon}_i$) is converted to the uniaxial strain rate $\dot{\varepsilon}_u$ by the empirical relation, $\dot{\varepsilon}_u \sim 0.01\dot{\varepsilon}_i$ (where $\dot{\varepsilon}_u$ is the uniaxial strain rate), found from a study of nc-Ni [3]. n can then be obtained from the slope of the near-end part (possibly corresponding to the steady-state condition) of the plot of log(stress) vs. log(strain rate). Note that the conversions to uniaxial stress and strain rate by the empirical relations do not affect the value of n due to the nature of logarithmic plotting.

Despite the popularity of the constant-load indentation creep method, the n values of nc materials estimated through these tests have been rather controversial. For example, Ma et al. [10,11] reported an n value in the range of 20–140 in nc-Ni with an average grain size of 25 nm. As pointed out in Ref. [9], n values of this magnitude seem to be too high and physically implausible for a creep-like process. This leads to an important question which is the principal motive of the present work: what factors in constant-load sharp-indentation creep are responsible for the measured n values? Here, we suggest some important essentials related to the self-similar geometry of a sharp tip. First, for both sharp and spherical indentation, the characteristic indentation strain ε_i (which is the strain comparable to uniaxial flow strain) is defined as $0.2\tan\beta$ [13], where β is the inclination of the indenter face to the sample surface. For a sharp tip, β and thus the strain are fixed and independent of creep displacement due to the geometrical self-similarity of the indenter, while the creep strain vs. time curve is the key data in uniaxial creep tests. Second, in terms of the continuum plasticity concept, the characteristic stress underneath a given sharp tip is unique, which makes it virtually impossible to plot the change in strain rate as a function of stress. Therefore, in this method, the change in displacement during the load–hold sequence is used to calculate the stress variation. It might be supposed this can be an advantage because the stress exponent can be predicted from a single test. However, it should be noted that, in the standard constant-load tension creep test, the applied stress values used for calculating n are not the stresses varying in the load–hold sequence but the initial stress at the onset of creep, and thus a large number of tests at different initial stress levels are required in order to determine the value of n. This concept cannot be applied in this method unless multiple tips having different angles are used for the experiments. Third, the unique characteristic stress must be plastic due to the singularity of the tip (if the tip is not blunted). This may result in a difference from the uniaxial creep data for which applied stress is elastic. Fourth, the presence of the indentation size effect (ISE, which is manifested as an increase in hardness with decreasing indentation depth for a sharp indentation [14]) can complicate the analysis of the stress–strain rate relationship. Last, but not the least, grain growth during creep testing is a major concern in nc materials when using a sharp tip [15]. Note that these issues raised here are only related to the tip geometry. We have excluded more fundamental issues such as the difference in stress state between uniaxial loading and indentation.

In this paper, we report a modified constant-load indentation creep test using a spherical indenter. The indentation strain ε_i $(= 0.2\tan\beta)$ can be rewritten as $0.2(a/R)$ [13], where a is the contact radius and R is the tip radius. For a fixed R, both ε_i and hardness H at the onset of creep can be systematically varied by simply changing the applied peak load, P_{max}. Thus, increasing P_{max} can lead to a dramatic increase in strain and stress from elastic to elastoplastic, and then to fully plastic regimes [13]. In addition, the ISE in spherical indentation is different from that in sharp indentation, i.e. the hardness is not significantly affected by the indentation depth h but by the tip radius R [14]. To examine the effectiveness of our approach, we performed constant-load nanoindentation creep experiments on nc-Ni using both a sharp and a spherical tip and directly compared the obtained n values.

The used material was electrodeposited nc-Ni foil of 150 μm thickness with an average grain size of 30 nm [16]. The surfaces of indentation samples were initially ground with SiC papers and polished with a microcloth using 0.3 μm alumina. Creep experiments were performed at room temperature (RT) using a Nanoindenter-XP (MTS Corp., Oak Ridge, TN) with two different indenters, i.e. a Berkovich tip and a spherical tip with $R = 30$ μm which was estimated by Hertzian contact analysis [13] of the indentations made on fused quartz. During nanoindentation creep testing, the specimen was loaded to different P_{max} at a constant loading rate (dP/dt) of 0.5 mN s^{-1}, held at P_{max} for 200 s, and fully unloaded. More than 10 tests were conducted for each testing condition, and the thermal drift was maintained below 0.05 nm s^{-1} in all experiments.

Figure 1 provides examples of the data obtained from the Berkovich indentation creep tests made at three different P_{max} (10, 50 and 100 mN). The strain rate obtained from these tests typically falls in the range of 10^{-6}–10^{-5} s^{-1}. It is noteworthy that C (for the conversion of hardness to stress) used here is 4 instead of 3,

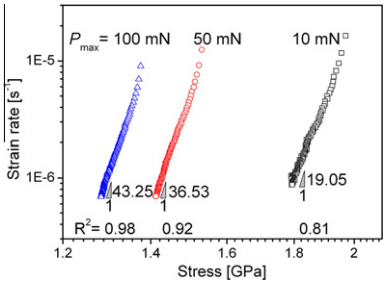

Figure 1. Some log(strain rate) vs. log(stress) plots from Berkovich indentation creep tests at different P_{max}.

according to the previous work on nc-Ni [17]. Similar to the previous data by Ma et al. [10,11], the estimated value of n is high and increases with P_{max}: n is 19.67 ± 6.66 for 10 mN, 35.37 ± 14.36 for 50 mN, and 38.16 ± 15.35 for 100 mN. The hardness at the onset of creep, roughly estimated as $P_{max}/(24.5h_0^2)$, where h_0 is the displacement at the start of the holding, is found to show a clear trend of ISE: 8.24 ± 0.09 GPa for 10 mN, 6.27 ± 0.05 GPa for 50 mN, and 5.47 ± 0.21 GPa for 100 mN. Therefore, it appears that n increases with decreasing stress. However, this cannot be explained by classical creep theory in which n becomes higher at higher stress regimes. Because of the clear ISE behavior and relatively high strain rates observed, we suggest that the widely used constant-load sharp nanoindentation test may not be the best approach to producing reliable creep data at RT, at least for the nc-Ni tested in this study.

Next, we attempted to estimate the value of n through modified constant-load nanoindentation creep experiments with a spherical indenter at eight different P_{max} (3, 5, 10, 20, 50, 100, 200 and 500 mN). The representative P–h curves recorded during the spherical indentation creep tests at different P_{max} are provided in Supplementary material (see Fig. S1). For all the cases of P_{max}, the penetration depth increases during the holding sequence, i.e. creep occurs. To classify the data from different P_{max} under the elastic and plastic regimes, we conducted normal quasi-static nanoindentation tests without peak-load holding. The normalized P–h curves are shown in the (left) inset of Figure S1. The loading and unloading parts of the P–h curves completely overlap for $P_{max} = 3$ and 5 mN (meaning deformation is purely elastic), whereas they do not overlap when P_{max} is over 10 mN, implying that yielding under quasi-static loading occurs at P_{max} between 5 and 10 mN. The typical P–h curve of indentation creep test at $P_{max} = 5$ mN is enlarged in the (right) inset of Figure S1. An increase in h during the holding sequence can be clearly seen, and this time-dependent deformation is not fully recovered upon unloading, suggesting that the observed creep behavior is mainly plastic in nature. From the Hertzian contact analysis [13] of the loading curve (see the right inset image of Fig. S1), the plane-strain modulus of the sample, $E_s/(1-\upsilon_s^2)$, where E_s and υ_s are Young's modulus and Poisson's ratio of the sample, respectively, was estimated to be 210 ± 9 GPa, which falls within the expected range given in the literature (150–220 GPa) [18]. This confirms that creep plasticity can be generated at RT even if the stress state underneath the indenter is less than the global yield strength.

Examples of the creep displacement Δh $(= h–h_0)$ vs. time curve are exhibited in Figure 2a, where it is clear that Δh increases with P_{max}. Figure 2b shows the total creep displacement h_{creep} (the maximum value of Δh at 200 s) is plotted as a function of P_{max}. In the elastic regime ($P_{max} = 3$ and 5 mN), the creep behavior is less pronounced and h_{creep} is below 3 nm. However, in the plastic regime, except for the case of $P_{max} = 10$ mN (which is close to the elastic regime and probably around the elastic-to-plastic transition regime), h_{creep} is relatively large and increases dramatically with indentation strain. Although the detailed mechanism for this small and stress-independent creep for $P_{max} \leqslant 10$ mN

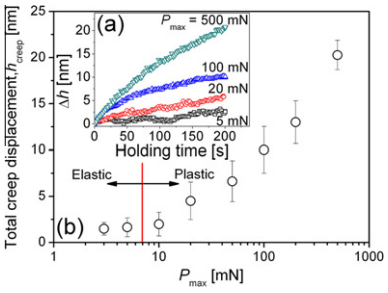

Figure 2. Typical results from spherical indentation creep: (a) creep displacement vs. time curves; (b) total creep displacement vs. peak load plots.

is not fully understood, one may gain a clue from the recent study of Wang et al. [19] who argued that, for shallow indentations, tip–sample interfacial diffusion dominates small volume creep deformation; but for deep indentations, conventional creep mechanisms related to microstructural activities are the dominant mechanism.

To quantitatively estimate n, the increased amount of indentation strain by creep was quantified as $0.2(a–a_0)/R$, where a_0 is the contact radius at the onset of creep. For this quantification, the contact radius a was calculated as $a = \sqrt{2hR - h^2}$. Figure 3a shows representative curves for the creep strain as a function of holding time. To estimate the indentation creep strain rates, we fitted the strain–time curves according to Garofalo's mathematical fitting equation originally suggested for conventional tensile creep analysis [7]:

$$\varepsilon = \varepsilon_0 + \alpha(1 - e^{-rt}) + \omega t, \tag{3}$$

where ε_0 is an instantaneous strain during loading (which is zero in Fig. 3a), α and ω are constants (whose physical meaning may be the limit of transient creep strain and the steady-state creep rate, respectively) and r is the ratio of transient creep rate to the transient creep

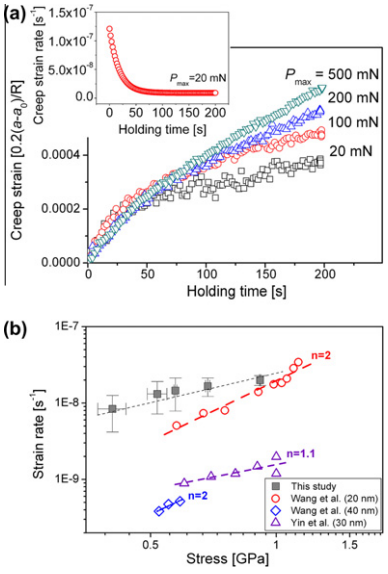

Figure 3. Examples of (a) creep strain vs. time curves (with inset image showing the strain rate vs. time data); (b) strain rate vs. stress relation to estimate the stress exponent n.

strain. We calculated the steady-state indentation strain rate $\dot{\varepsilon}_i$ by differentiating each fitting equation and averaging the values for the holding time between 180 and 200 s. An example of the strain rate vs. time plot in the inset of Figure 3a suggests the possibility of approaching close to the steady-state condition, although it is theoretically implausible to reach the steady-state condition during indentation creep [3,20]. Note that the strain rates ($\sim 10^{-8}\ s^{-1}$) we observed here are several orders of magnitude lower than those in sharp indenter experiments.

The final step was plotting the creep strain rate against the applied stress on a logarithmic scale, and calculating the stress exponent n from a slope of $\log(\dot{\varepsilon})$ and $\log(\sigma)$, as shown in Figure 3b. In the figure, the applied stress and the strain rate are converted from the hardness at the onset of creep H_0 by $\sigma \sim H_0/4 = P_{max}/4\pi a_0^2$ and the indentation strain rate by $\dot{\varepsilon}_u \sim 0.01\dot{\varepsilon}_i$ [3], respectively. We note again that these conversions do not affect the value of n. In addition, in the calculation of n, the data for the regime of $P_{max} \leqslant 10$ mN was not considered, since the creep for the regime might be controlled principally by vacancy diffusion along the tip–sample interface instead of conventional creep mechanisms, as mentioned before [19]. From a linear fitting of the "average points" for each P_{max} in Figure 3b, the creep stress exponent n is determined as 1.02146 (correlation factor $R^2 = 0.9583$). However, we found that the data fluctuate in the low-stress regime, which could lead to a higher n value of 1.8497 ($R^2 = 0.9638$).

In order compare our results with those in the literature, we notice (to the best of our knowledge) that only two original papers have reported the RT creep stress exponent of nc-Ni based on conventional uniaxial tensile creep experiments. Those data are shown in Figure 3b and are also included in Table S1 (in Supplementary material) together with other important creep results obtained for various nc-Ni samples. At RT, Wang et al. [6] reported $n \approx 1.18$ for a grain size, d, of 6 nm, $n \approx 2$ for both $d = 20$ and 40 nm (low stress case), and $n \approx 5.3$ for $d = 40$ nm (high-stress case), while Yin et al. [21] found $n \approx 1.1$ for 30 nm nc-Ni. The n value from our spherical indentation creep is similar to these data. Importantly, the strain rate achieved through spherical indentation is approximately the same as those obtained from uniaxial measurements, suggesting that at such slow strain rates ($<10^{-7}\ s^{-1}$), the deformation of nc-Ni is likely dominated by GB sliding or diffusion mechanisms. On the other hand, relatively higher strain rates ($\sim 10^{-5}$–$10^{-4}\ s^{-1}$), intrinsically associated with Berkovich indentations, imply that the steady-state creep region is unlikely to have reached in those experiments. Nonetheless, the resulting n values from Berkovich indentations are similar to those ($n = 1/m = \sim 50$, where m is the strain-rate sensitivity) obtained from uniaxial tension stress-relaxation experiments [16], which explore the strain-rate regime that is dictated by dislocation mechanisms. Overall, our Berkovich and spherical indentations indicate that at RT the n and m (see Table S1) of nc-Ni are strongly strain-rate dependent, i.e. m increases with decreasing strain rates—a general trend that is consistent with those reported in the literature for face-centered cubic nc metals (see Table S1 and Ref. [22]), suggesting that the deformation mechanism in nc-Ni is strain-rate dependent. Our results further indicate that the spherical indentation creep test is a better approximation for evaluating the steady-state creep stress exponent than the popular sharp indentation creep test.

This research was supported by Basic Science Research Program through the National Research Foundation of Korea (NRF) funded by the Ministry of Education, Science and Technology (No. 2010-0025526), and in part by the Human Resources Development of the Korea Institute of Energy Technology Evaluation and Planning (KETEP) grant funded by the Korea government Ministry of Knowledge Economy (No. 20101020300460). The work at Lawrence Livermore National Laboratory was performed under the auspices of the US Department of Energy under Contract DE-AC52-07NA27344.

Supplementary data associated with this article can be found, in the online version, at doi:10.1016/j.scriptamat.2011.04.031.

[1] S.X. McFadden, R.S. Mishra, R.Z. Valiev, A.P. Zhilyaev, A.K. Mukherjee, Nature 398 (1999) 684.
[2] K. Zhang, J.R. Weertman, J.A. Eastman, Appl. Phys. Lett. 85 (2004) 5197.
[3] C.L. Wang, M. Zhang, T.G. Nieh, J. Phys. D 42 (2009) 115405.
[4] C.L. Wang, Y.H. Lai, J.C. Huang, T.G. Nieh, Scripta Mater. 62 (2010) 175.
[5] R.S. Kottada, A.H. Chokshi, Scripta Mater. 53 (2005) 887.
[6] N. Wang, Z.R. Wang, K.T. Aust, U. Erb, Mater. Sci. Eng. A 237 (1997) 150.
[7] G.E. Dieter, Mechanical Metallurgy, McGraw-Hill, London, 1988.
[8] B.N. Lucas, W.C. Oliver, Metall. Mater. Trans. A 30 (1999) 601.
[9] R. Goodall, T.W. Clyne, Acta Mater. 54 (2006) 5489.
[10] Z.S. Ma, S.G. Long, Y. Pan, Y.C. Zhou, J. Mater. Sci. 43 (2008) 5952.
[11] Z.S. Ma, S.G. Long, Y.C. Zhou, Y. Pan, Scripta Mater. 59 (2008) 195.
[12] D. Tabor, J. Inst. Met. 79 (1951) 1.
[13] K.L. Johnson, Contact Mechanics, Cambridge University Press, Cambridge, 1985.
[14] G.M. Pharr, E.G. Herbert, Y.F. Gao, Ann. Rev. Mater. Res. 40 (2010) 271.
[15] K. Zhang, J.R. Weertman, J.A. Eastman, Appl. Phys. Lett. 87 (2005) 061921.
[16] Y.M. Wang, A.V. Hamza, E. Ma, Acta Mater. 54 (2006) 2715.
[17] I. Brooks, P. Lin, G. Palumbo, G.D. Hibbard, U. Erb, Mater. Sci. Eng. A 491 (2008) 412.
[18] K.S. Siow, A.A.O. Tay, P. Oruganti, Mater. Sci. Technol. 20 (2004) 285.
[19] F. Wang, P. Huang, T. Lu, J. Mater. Res. 24 (2009) 3277.
[20] C.D. Gu, J.S. Lian, Q. Jiang, W.T. Zheng, J. Phys. D 40 (2007) 7440.
[21] W.M. Yin, S.H. Whang, R. Mirshams, C.H. Xiao, Mater. Sci. Eng. A 301 (2001) 18.
[22] Y.M. Wang, E. Ma, Acta Mater. 52 (2004) 1699.